arXiv:1303.7447v1 [cond-mat.mes-hall] 29 Mar 2013

Emergence of Majorana modes in cylindrical nanowires

Jong Soo Lim[1], Rosa Lopez[1,2] and Llorenç Serra[1,2]

[1] *Institut de Fisica Interdisciplinària i de Sistemes Complexos IFISC (CSIC-UIB), E-07122 Palma de Mallorca, Spain*
[2] *Departament de Fisica, Universitat de les Illes Balears, E-07122 Palma de Mallorca, Spain*

PACS `73.63.-b` – Condensed Matter: Electronic Structure, Electrical, Magnetic
PACS `73.50.Fq` – High-field and nonlinear effects

Abstract –We present calculations of Majorana edge modes in cylindrical nanowires of a semiconductor material with proximity-induced superconductivity. We consider a Rashba field along the transverse direction and an applied magnetic field in arbitrary orientation. Our analysis is based on exact numerical diagonalizations for the finite cylinder and on the complex band structure for the semi-infinite one. Orbital effects are responsible for a strong anisotropy of the critical field for which the effective gap vanishes. Robust Majorana modes are induced by the parallel field component and we find regimes with more than one Majorana mode on the same edge. Experimentally, they would manifest as a specific sequence of zero-bias conductances as a function of magnetic field. In the finite cylinder, a degradation of the Majorana modes due to interference of the two edges leads to oscillating non zero energies for large enough fields.

Introduction. – Novel states of matter, such as quantum Hall systems [1–4], obey topological rules. The advent of topological materials [5–8] was a major breakthrough towards the achievement of a topological quantum computer. In these materials, quasiparticles are non Abelian composite fermions [9–11], the potential basic units for quantum information processing [12]. Such peculiar excitations are identical to their own antiparticles and they are termed Majorana fermions (MFs) honouring Ettore Majorana who predicted their existence in 1937.

Majorana's original aim was to explain the nature of neutrinos as real solutions of the Dirac equation for relativistic particles [13–17]. Notoriously, there is not yet a conclusive clue on the existence of MFs as elementary particles but they have been engineered in a laboratory as quasiparticles. Majorana fermions in topological materials can be described as half-fermionic states, so that a pair of MFs forms a widely distributed full-fermionic state. A pair of MFs defines a qubit whose information is encoded not in the individual particles but in a non local pair of identical and neutral entities. Non locality gives a great advantage to such pairs, they are immune against local sources of decoherence. Majorana fermions are incredibly elusive because of their lack of characteristic features. They are chargeless, spinless and energyless, what makes them difficult to detect.

The discovery of topological systems brought different proposals for the physical realization of MFs in solid state devices [17–20]. Recently, they have been proposed in semiconductor nanowires as a combined effect of superconductivity, spin-orbit interaction and magnetic field [21–23]. Mourik and coworkers reported in Ref. [24] signatures of such quasiparticles in long InSb nanowires ($L \approx 2\mu$m). In the experimental setup an InSb nanowire is connected to a normal-metal gold electrode on one side and to a superconducting niobium titanium nitride electrode on the other. Since the NbTiN contact is brought in close proximity to the InSb nanowire, leakage of Cooper pairs induces superconductivity, at least over a coherence length of a few hundred nanometers. InSb is characterized by a large g factor, so that the application of an ex-

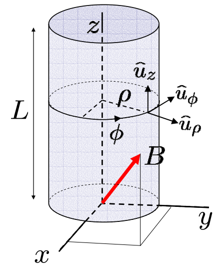

Fig. 1: Hollow semiconductor nanowire with cylindrical geometry of length L. Cylindrical coordinates and unit vectors are indicated. A magnetic field $\vec{B}$ is applied in an arbitrary direction.

ternal magnetic field closes the superconductor gap, shifting some states to zero energy. The spin-orbit interaction induces anticrossings that separate the zero energy state from the nearest excited states, preventing the decoherence of the Majorana mode. The Majorana-mode evidence is a robust zero bias peak in the tunneling differential conductance, a zero-bias anomaly (ZBA), when the nanowire is magnetically driven into the topological phase.

More experiments have reported evidence of Majorana modes in nanowires. Deng *et al.* have also observed a ZBA in the nonlinear transport measurements with an InSb nanowire quantum dot [25]. Almost simultaneously, Das *et al.* provided similar evidences in shorter hybrid semiconductor/superconductor InAs/Al nanowire junctions [26]. Rokhison and coworkers [27] have presented indirect measurements of the fractional a.c. Josephson effect in hybrid InSb/Nb nanowire junctions as a hallmark of the topological matter. A more recent experiment by Finck *et al.* [28] demonstrates a striking effect: the splitting of the ZBA at high magnetic field and its oscillatory evolution, in agreement with the theoretical expectations [29, 30].

From the theoretical side, most works dealing with Majorana physics in hybrid semiconductor/superconducting nanowires assume planar geometries. However, all the above mentioned experiments are done with cylindrical nanowires. This motivates us to investigate the theory of Majorana edge modes in cylinders. We quantify the importance of the cylindrical configuration, rather than a planar one, regarding the different influence of both Rashba field and orbital magnetic effects.

We find that in cylinders a fixed Rashba direction has to be assumed, since a radial one does not favour the formation of Majoranas. Orbital effects are inevitably present, however, we demonstrate that they are less dramatic in cylindrical nanowires than in planar ones. In the latter, a slight deviation of the magnetic field from the nanowire plane completely destroys the Majorana state [29]. Remarkably, orbital effects drive the cylinder into new topological phases in which several Majorana modes can coexist on the same edge. We predict the specific sequence of topological phases in parallel field for finite and semi-infinite cylinders. Besides, we show that the critical field for gap closing strongly depends on the magnetic field orientation due to the presence of orbital effects.

Model. – We study the spectrum of a semiconductor nanowire with cylindrical shape in a magnetic field. The quasiparticles are assumed to move only on the surface of the cylinder, with a total Hamiltonian $\mathcal{H} = \mathcal{H}_{kin} + \mathcal{H}_R + \mathcal{H}_Z + \mathcal{H}_{pair}$, where the successive contributions are kinetic, Rashba spin-orbit, Zeeman, and pairing ones. We include the orbital effects of the magnetic field in the kinetic and Rashba Hamiltonians via their dependence on quasiparticle momentum. The electron and hole degrees of freedom are represented, as usual, with Pauli matrices $\tau_{x,y,z}$ acting in the so-called Nambu space.

The kinetic energy is split into non-magnetic and magnetic terms as $\mathcal{H}_{kin} = \mathcal{H}_{kin}^{(0)} + \mathcal{H}_{kin}^{(1)}$, where

$$\begin{aligned}
\mathcal{H}_{kin}^{(0)} &= \left[\frac{p_\phi^2 + p_z^2}{2m^*} - \mu\right]\tau_z\ , &(1)\\
\mathcal{H}_{kin}^{(1)} &= \frac{\hbar^2}{2m^*}\left[\frac{\rho}{\ell_z^2}\frac{p_\phi}{\hbar}\tau_z + \frac{\rho^2}{4\ell_z^4}\tau_z\right.\\
&+ 2\frac{\rho}{\ell_x^2}\sin\phi\,\frac{p_z}{\hbar}\tau_z - 2\frac{\rho}{\ell_y^2}\cos\phi\,\frac{p_z}{\hbar} + \frac{\rho^2}{\ell_x^4}\sin^2\phi\,\tau_z\\
&+ \left.\frac{\rho^2}{\ell_y^4}\cos^2\phi\,\tau_z - 2\frac{\rho^2}{\ell_x^2\ell_y^2}\sin\phi\cos\phi\right]\ . &(2)
\end{aligned}$$

We employ the cylindrical coordinate system indicated in Fig. 1 and denote the chemical potential by μ and the magnetic length along a general direction $a = x, y, z$ by $\ell_a = \sqrt{\hbar c/eB_a}$. Notice that, trivially, when a certain field component vanishes the corresponding magnetic length diverges, giving a vanishing contribution to $\mathcal{H}_{kin}^{(1)}$.

The Rashba Hamiltonian originates in an *effective* electric field $\vec{\mathcal{E}}$ as $\mathcal{H}_R \propto \vec{\sigma}\cdot(\vec{p}\times\vec{\mathcal{E}})$. We initially considered a radial field $\vec{\mathcal{E}} = \mathcal{E}\hat{u}_\rho$ but, since this does not lead to the appearance of any Majorana states, we finally assumed a uniform direction $\vec{\mathcal{E}} = \mathcal{E}\hat{u}_x$. Similarly to the kinetic term, we write $\mathcal{H}_R = \mathcal{H}_R^{(0)} + \mathcal{H}_R^{(1)}$, with

$$\begin{aligned}
\mathcal{H}_R^{(0)} &= \frac{\alpha}{\hbar}\left[p_z\sigma_y\tau_z - \cos\phi\, p_\phi\sigma_z - \frac{i\hbar}{2\rho}\sin\phi\,\sigma_z\right]\ , &(3)\\
\mathcal{H}_R^{(1)} &= \alpha\left[\frac{\rho}{\ell_x^2}\sin\phi\,\sigma_y\tau_z - \frac{\rho}{\ell_y^2}\cos\phi\,\sigma_y\right.\\
&\qquad\left. - \frac{\rho}{2\ell_z^2}\cos\phi\,\sigma_z\right]\ . &(4)
\end{aligned}$$

The Zeeman contribution reads

$$\mathcal{H}_Z = \Delta_B\vec{\sigma}\cdot\hat{n}\ , \tag{5}$$

where $\hat{n}$ gives the direction of the magnetic field and parameter Δ_B is related to the gyromagnetic factor g by $\Delta_B = g\mu_B B/2$. The final Hamiltonian contribution is the superconductivity (pairing) one

$$\mathcal{H}_{pair} = \Delta_0\tau_x\ . \tag{6}$$

In summary, the Hamiltonian depends on the field orientation $\hat{n}$, as well as on parameters Δ_0, Δ_B and α representing the superconducting, Zeeman and Rashba coupling strengths, respectively. In order to investigate realistic setups we assume parameter values from Ref. [24]. The effective mass, Rashba spin-orbit coupling, and radius of InSb nanowire are $m^* = 0.015m_e$ (m_e is the electron bare mass), $\alpha \approx 0.2$ eVÅ and $\rho \approx 50$ nm. A convenient choice of energy and length units is then

$$\begin{aligned}
E_U &\equiv \frac{\hbar^2}{m^*\rho^2} = 2.03\,\text{meV}\ ,\\
L_U &\equiv \rho = 50\,\text{nm}\ . &(7)
\end{aligned}$$

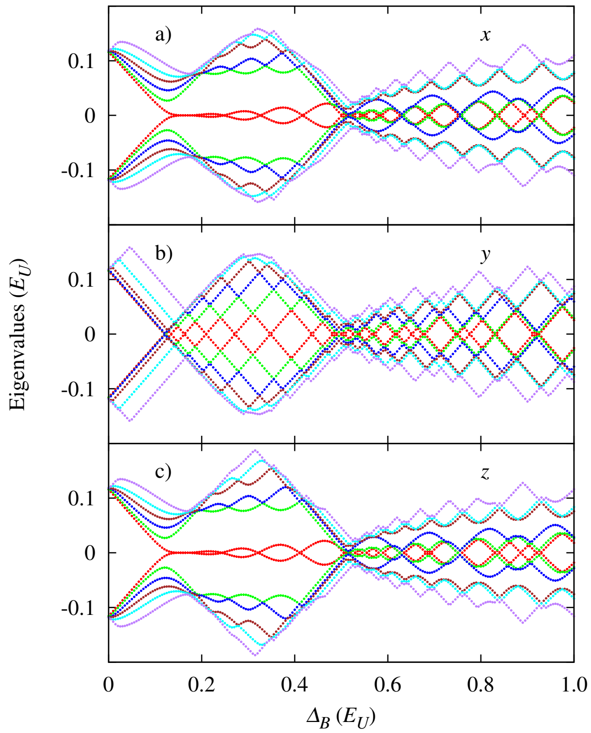

Fig. 2: Eigenvalues vs Δ_B when orbital effects are omitted. Panels (a), (b) and (c) correspond to applied magnetic fields pointing along x, y and z, respectively. x and z directions are almost identical. Parameters: $\Delta = 0.12E_U$, $\alpha = 0.2E_U L_U$, $\mu = 0E_U$, $\rho = L_U$, and $L_z = 30L_U$. Number of basis: $N_n = 51$ and $N_m = 31$. Only the twelve eigenvalues closer to zero energy have been displayed.

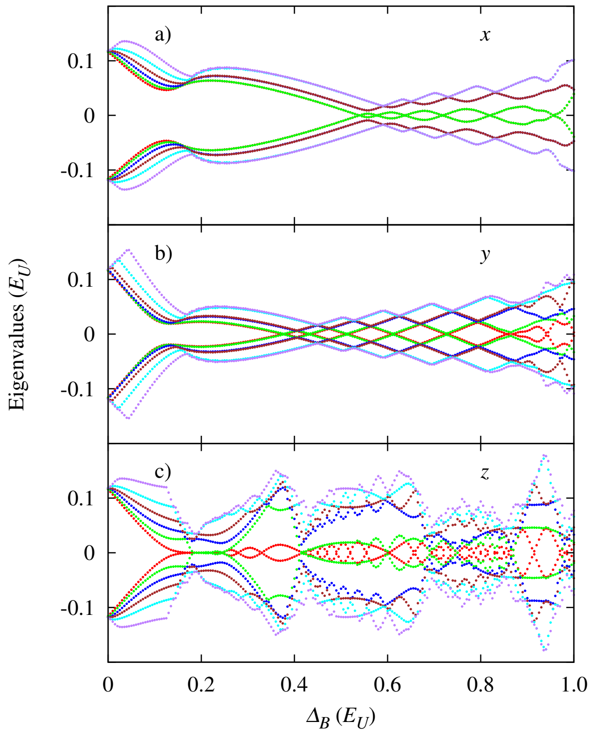

Fig. 3: Same as Fig. 2 with orbital effects.

We also consider a superconducting parameter $\Delta_0 \approx 0.25$ meV and a Zeeman energy that for $g \approx 50$ is related to the field B by $\Delta_B = 0.723B\mathrm{T}^{-1}E_U$.

Finite cylinders. – We have performed numerical diagonalizations of the Hamiltonian for a cylinder of length L using as a basis states $|nms_\sigma s_\tau\rangle$, where $n = 1, 2, \ldots$ represent square well eigenstates (z motion), $m = 0, \pm 1, \pm 2, \ldots$ represent L_z angular momentum eigenstates (ϕ motion) while $s_\sigma = \pm$ and $s_\tau = \pm$ are the usual spin and isospin two component eigenstates.

Figures 2 and 3 show the energy spectrum of a long cylindrical nanowire ($L = 30L_U$) when the magnetic field is applied along the three Cartesian axis. In Fig. 2 orbital effects have been neglected ($\ell_{x,y,z} = \infty$) while in Fig. 3 the full Hamiltonian is considered. For the $\hat{y}$ direction the spectrum in Fig. 2b is dense, with accidental crossings at zero energy but no robust Majorana modes. Field orientations along $\hat{x}$ and $\hat{z}$ (Figs. 2a and 2c) are basically equivalent and they show the emergence of a zero energy (Majorana) mode beyond a critical field $\Delta_B^{(c)} = 0.15E_U$. Right after the critical field a clear energy gap separates this mode from other excitations. However, as Δ_B increases an enhanced oscillating behavior manifests the degradation of the Majorana mode. This is a finite size effect and agrees with our previous study of planar geometries [29] as well as with Ref. [30]. Importantly, recent experimental evidences have confirmed this remarkable dependence of the Majorana pair splitting by measurements of the tunneling differential conductance [28]. When Δ_B exceeds $0.5E_U$ two more modes emerge in Fig. 2a and 2c; i.e., a total of three Majorana modes are oscillating around zero energy. Labeling each topological phase of the cylinder by the number of different Majorana modes the expected sequence when increasing the magnetic field is then $0 - 1 - 3 - \ldots$. Each m-subset contributes an independent Majorana after some critical field, while degeneracy of m and $-m$ causes modes to emerge in pairs, except for $m = 0$. We focus next on the changes to this scenario induced by orbital effects.

Figure 3 shows the influence of orbital effects on the nanowire energy spectrum. Now $\hat{x}$ and $\hat{z}$ orientations are no longer equivalent and a large anisotropy in the gap-closing field is obtained. This critical field is strongly reduced along the sequence $x \to y \to z$. Along $\hat{x}$ (Fig. 3a) a state of unclear Majorana character emerges beyond $\Delta_B \approx 0.5E_U$, with an oscillating energy and nearby excited modes. For the $\hat{z}$ direction (Fig. 3c) a clear Majorana mode emerges at a much lower magnetic field, $\Delta_B \approx 0.15E_U$. Interestingly, when increasing the field along $\hat{z}$ a second Majorana mode seems to be present for $0.18E_U < \Delta_B < 0.27E_U$. This behavior is in sharp contrast with planar geometries, where Rashba mixing precludes the coexistence of more than one Majorana mode. In cylinders, Rashba mixing is effectively weaker,

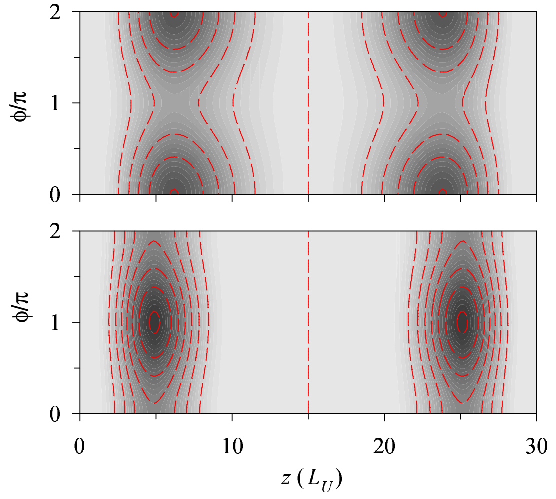

Fig. 4: Density distributions corresponding to the two Majorana modes of Fig. 3c with $\Delta_B = 0.2E_U$. An arbitrary gray colour scale is used, with dark colour indicating higher density.

as its strength changes sign with the azimuthal angle [cf. Eqs. (3) and (4)]. Notice also that the spin-orbit length, $L_{SO} = \hbar^2/m\alpha \approx 250$ nm, is $L_{SO} >> \rho$, also indicating a regime of weak spin-orbit where multiple Majoranas may coexist [31]. Increasing further the magnetic field in Fig. 3c, oscillations around zero energy become large and the Majorana character of the states is blurred. The sequence of topological phases as the field is increased suggested in Fig. 3c is $0-1-2-1-2-3-2$. This is in clear difference with the findings in absence of orbital effects, Fig. 2c.

In transport measurements, the presence of multiple Majorana modes affects the zero-bias conductance G_0. More precisely, $G_0 = M\mathcal{G}$, where M is the number of Majorana modes and $\mathcal{G}$ is a quantization unit depending on the nature of the contacts ($\mathcal{G} = 2e^2/h$ for a normal-superconductor junction). Although, currently, experiments are still far from this limit of high conductances [32], the observation of a zero bias conductance following the above sequence with magnetic field would be a clear proof of the cylinder topological phases.

As an illustrative case, Fig. 4 shows the densities of the two Majorana modes of Fig. 3c when $\Delta_B = 0.2E_U$. As expected, the densities are localized close to the cylinder edges and decay towards the central part. Remarkably, however, the density maxima of the two modes take complementary azimuthal positions, indicating an effective repulsion between Majorana modes. We have also obtained that when the mode energies deviate from zero due to the finite size effect, for large Δ_B's, the densities extend more towards the centre, eventually occupying all of the cylinder length.

Semi-infinite cylinders. – The above results show that finite size effects are relevant for an aspect ratio $L/\rho = 30$. We have checked that for $L/\rho = 60$ (results not shown) the finite size oscillations are reduced but the behavior is qualitatively the same at high fields. Therefore, in order to ascertain the sequence of topological phases mentioned above, we have directly addressed the semi-infinite cylinder using the complex band structure approach of Ref. [33]. In the semi-infinite system there is a single edge, the other one lying at infinite distance, and finite-size artifacts are absent by definition.

For a complex wave number k the eigenstate of the infinite-cylinder Hamiltonian reads

$$\Psi_k(z,\phi,\eta_\sigma,\eta_\tau) = e^{ikz} \sum_{s_\sigma s_\tau} \psi^{(k)}_{s_\sigma s_\tau}(\phi)\, \chi_{s_\sigma}(\eta_\sigma)\, \chi_{s_\tau}(\eta_\tau)\ , \quad (8)$$

where, generically, $\eta_{\sigma,\tau} = \uparrow,\downarrow$ refers to a spin-isospin discrete variable and $s_{\sigma,\tau} = \pm$ is the corresponding quantum number. We have determined the allowed wave numbers k and state amplitudes $\psi^{(k)}_{s_\sigma s_\tau}$ for a given energy using the approach of Ref. [33]. A Majorana mode is signaled by a zero eigenvalue in matrix

$$\mathcal{M}_{kk'} = \sum_{s_\sigma s_\tau} \int d\phi\, \psi^{(k)*}_{s_\sigma s_\tau}(\phi)\, \psi^{(k')}_{s_\sigma s_\tau}(\phi)\ . \quad (9)$$

In practice the set of complex wave numbers is truncated to a finite size using a cut-off in momentum and the emergence of a zero eigenvalue of matrix $\mathcal{M}$ is actually seen as a steadily decreasing eigenvalue with increasing value of the cut-off. The approach of Ref. [33] provides also a method to obtain the critical fields corresponding to phase transitions. They are seen as zeros in function $\mathcal{F}(\Delta_B)$, the derivative discontinuity at an arbitrary matching point for $k = 0$.

Figure 5 confirms the scenario inferred above from the finite cylinder calculations. Remarkably, the sequence of nodes in $\mathcal{F}$ (Fig. 5a) has a clear correspondence with the changes in the finite cylinder spectrum of Fig. 3c. In the semi-infinite cylinder the critical fields for topological transitions can be determined accurately, while in the finite cylinder transitions are blurred, specially at high fields. Lower panels in Fig. 5 contain the evolution with cut-off in wave numbers of the eigenvalues of matrix $\mathcal{M}$. In the first region ($\Delta_B < 0.15E_U$) the lowest eigenvalue converges to ≈ 1, indicating that no edge mode is possible. In the second and third regions we see that one and two eigenvalues, respectively, keep decreasing as the cut-off is increased. This is a clear evidence that second and third regions contain one and two Majorana modes, respectively. Similar plots (not shown) are obtained for the successive regions, containing the number of Majoranas indicated in Fig. 5a. Topological invariance is manifested as independence of the number of Majorana modes with the precise value of Δ_B, as long as this remains within a given interval between nodes of Fig. 5a.

The spatial densities of the two Majorana modes for $\Delta_B = 0.2E_U$ are shown in Fig. 6. When compared with the finite cylinder, densities are in good agreement for cases when the finite-cylinder mode is very close to zero energy. If not, large discrepancies in the bulk of the

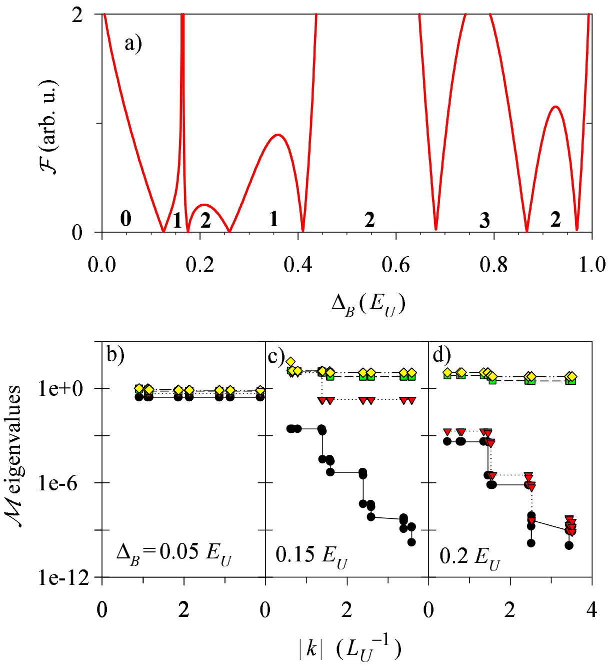

Fig. 5: Upper panel: function $\mathcal{F}$ whose nodes signal the topological transitions. The number of Majorana edge states are indicated for the low field regions. Lower panels: Evolution of matrix $\mathcal{M}$ eigenvalues with the cut-off in wave numbers (in absolute value). Each eigenvalue tending to zero in the limit of large $|k|$'s corresponds to a Majorana mode. Except for the infinite cylinder length all other parameters are the same of Fig. 2c.

cylinder are found. An obvious difference, of course, is that in the finite cylinder the density is repeated on the two edges. A similar avoided mode overlap is found in both cases, and there is only a minor angular shift in the relative position of the maxima. We finally mention that the wave function of Majorana modes is quasi-real, i.e., its imaginary part almost vanishes. The wave function is more real the more k's are included in its expansion, and fulfills $\Psi(z,\phi,\uparrow,\uparrow) = -\Psi(z,\phi,\downarrow,\downarrow)$ and $\Psi(z,\phi,\uparrow,\downarrow) = \Psi(z,\phi,\downarrow,\uparrow)$. Both things are to be expected for proper Majorana solutions.

Conclusions. – In closing, we have investigated the occurrence of Majorana zero-energy modes at the edges of cylindrical nanowires using both finite and semi-infinite models. We have considered a Rashba field along $\hat{x}$ and a magnetic field in arbitrary direction. Under this situation we report the strong influence of the orbital effects on the appearance of zero energy states. First, the critical fields corresponding to gap closings strongly depend on the magnetic field orientation. Second, in contrast with planar geometries we observe phases where several Majorana modes coexist. Orbital effects define the sequence of phases with increasing field. The observation of the sequence $0-1-2-1-2-3\ldots$ in the zero bias conductance as a function of magnetic field (in units of the conductance quantum) would be a clear manifestation of the cylinder topological phases. As in planar geometries, at high fields an oscillating behavior signals the degradation of the Majorana character due to finite size effects.

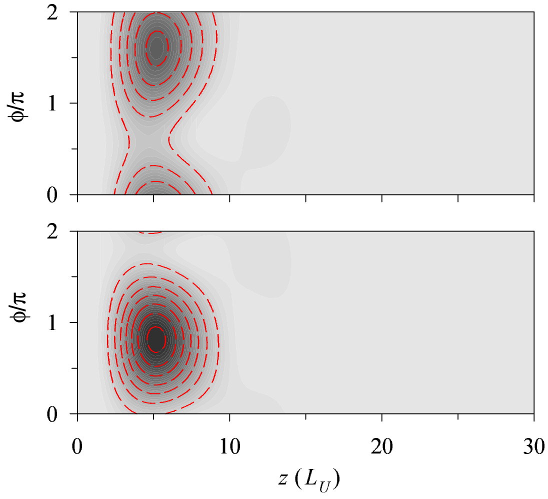

Fig. 6: Density distributions corresponding to the two Majorana modes of a semi-infinite cylinder with $\Delta_B = 0.2E_U$. All other parameters are the same of Fig. 2c.

* * *

Work supported by MINECO Grants No. FIS2011-23526, CSD2007-00042 (CPAN), the Conselleria d'Educació, Cultura i Universitats (CAIB) and FEDER.

REFERENCES

[1] Ando T., Matsumoto Y. and Uemura T., *J. Phys. Soc. Jpn.*, **39** (1975) 279.
[2] Klitzing K., Dorda D. and Pepper M., *Phys. Rev. Lett.*, **45** (() 1980)494.
[3] Laughlin R. B., *Phys. Rev. B*, **23** (1981) 5632.
[4] Yennie D. R., *Rev. Mod. Phys.*, **59** (1987) 781.
[5] Kane C.L and Mele E.J, *Phys. Rev. Lett.*, **95** (2005) 14680.
[6] Bernevig B. A., Taylor L. H. and Shou-Cheng Z., *Science*, **314** (2007) 5806.
[7] König J., Wiedmann S., Brüne C., Roth A., Buhmann H., Molenkamp L. W., Qi X.-L. and Zhang S.-C., *Science*, **318** (2007) 5851.
[8] Hasan M. Z. and Kane L., *Rev. Mod. Phys.*, **82** (2010) 3045.
[9] Wilczek F., *Phys. Rev. Lett.*, **49** (1982) 957.
[10] Moore G. and Read N., *Nuclear Physics B*, **360** (1991) 362.
[11] Stern A., *Nature*, **464** (2010) 187.
[12] Nayak C., Stern A., Freedman M. and Das Sarma S., *Rev. Mod. Phys.*, **80** (2008) 1083.
[13] Wilczek F., *Nature Phys.*, **5** (2009) 614.
[14] Kopnin N. B. and Salomaa M. M., *Phys. Rev. B*, **44** (1991) 9667.
[15] Volovik G.E., *JETP Letters*, **70** (1999) 609.

[16] Read N. and Green D., *Phys. Rev. B*, **61** (2000) 10267.
[17] Kitaev A. Yu., *Physics-Uspekhi*, **44** (2001) 131.
[18] Beenakker C., *arXiv:1112.1950*, **2012** (.)
[19] Alicea J., *arXiv:1202.1293*, **2012** (.)
[20] Fu L. and Kane C. L., *Phys. Rev. Lett.*, **100** (2007) 096407.
[21] Alicea J., *Phys. Rev. B*, **81** (2010) 125318.
[22] Lutchyn R. M., Sau J. D. and Das Sarma S., *Phys. Rev. Lett.*, **105** (2010) 077001.
[23] Oreg Y., Refael G. and Von Oppen F., *Phys. Rev. Lett.*, **105** (2010) 177002.
[24] Mourik V., Zuo K., Frolov S. M., Plissard S. R., Bakkers E. P. A. M. and Kouwenhoven L. P., *Science*, **336** (2012) 1003.
[25] Deng M. T., Yu C. L., Huang G. Y., Larsson P., Caroff M. and Xu H. Q., *arXiv:1204.4130*, **2012** (.)
[26] Das A., Ronen Y., Most Y., Oreg Y., Heiblum M. and Shtrikman H., *arXiv:1205.7073*, **2012** (.)
[27] Rokhinson L.P, Liu X. and Furdyna J. K., *Nature Physics*, **10** (2012) 1038.
[28] Finck A. D. K., Van Harlingen D. J., Mohseni P. K., Jung K. and Li X., *arXiv:1212.1101*, **2012** (.)
[29] Lim J. S., Serra L., López R. and Aguado R., *Phys. Rev. B*, **86** (2012) 121103.
[30] Das Sarma S., Sau J. D. and Stanescu T. D., *Phys. Rev. B*, **86** (2012) 220506.
[31] Stanescu T.D., Lutchyn R.M. and Das Sarma S., *Phys. Rev. B*, **87** (2013) 094518.
[32] Franz M., *Nature Nanotech.*, **8** (2013) 149.
[33] Serra L., *Phys. Rev. B*, **87** (2013) 075440.